Vol. 700: 179–196, 2022
https://doi.org/10.3354/meps14168

MARINE ECOLOGY PROGRESS SERIES
Mar Ecol Prog Ser

Published November 10

Hatching distribution, abundance, and losses to freshwater diversions of longfin smelt inferred using hydrodynamic and particle-tracking models

Edward Gross[1,*], Wim Kimmerer[2], Josh Korman[3], Levi Lewis[4], Scott Burdick[1], Lenny Grimaldo[5]

[1]Resource Management Associates Inc., Davis, CA 95618, USA
[2]Estuary & Ocean Science Center, San Francisco State University, Tiburon, CA 94920, USA
[3]Ecometric Research, Vancouver, BC V6S 1J3, Canada
[4]Wildlife, Fish and Conservation Biology, University of California Davis, Davis, CA 95616, USA
[5]California Department of Water Resources, Sacramento, CA 94236, USA

ABSTRACT: The distribution of larval fishes is influenced by where they hatch and their movements after hatching. In the San Francisco Estuary, the threatened longfin smelt *Spirinchus thaleichthys* spawns adhesive eggs in fresh to brackish water. Attached eggs hatch and the larvae disperse seaward toward higher-salinity water. Actual locations of spawning and hatching are unknown, and cannot reliably be inferred from distributions of larvae because intense tidal mixing obscures the history of movement. Human interventions such as manipulations and diversions of freshwater flow may contribute to the ongoing decline of this species, and these effects depend on where the fish hatch. We combined movement estimated using hydrodynamic and particle-tracking modeling with trawl data using a Bayesian model to estimate the location and timing of hatching, as well as natural mortality of larvae and losses to freshwater diversions. Results indicate that longfin smelt may hatch further seaward than previously believed, and that estimated direct losses due to diversions were small relative to other sources of mortality. Abundance of this species varies ~100-fold with freshwater flow, but our results suggest that proportional entrainment was practically zero during an extreme wet year and relatively low (2%) in a moderately dry year. This method could be applied to other estuarine and coastal systems where strong mixing reduces the ability of simpler models to predict hatching locations and larval movements.

KEY WORDS: Longfin smelt · *Spirinchus thaleichthys* · Osmerid · Larval transport · San Francisco Estuary · Survival · Particle tracking · Bayesian analysis

1. INTRODUCTION

Migratory estuarine and coastal fish larvae disperse from hatching locations in coastal and estuarine environments before a fraction of them recruit to suitable habitats for development as juveniles (Bradbury et al. 2006). The timing and distribution of hatching and subsequent hydrodynamic conditions experienced by larvae influence their dispersal and likelihood of recruitment (Bradbury et al. 2000). Therefore, quantifying the timing and distribution of hatching can allow improved environmental management using tools such as manipulation of freshwater flows to the estuary and targeted habitat restoration to improve recruitment (Grimaldo et al. 2017).

Hatching distribution and subsequent larval distribution and movement have been inferred in several ways. Larvae have been captured in trawl sur-

*Corresponding author: ed@rmanet.com

veys to assess larval distribution over space and time (Grimaldo et al. 2020). However, survey data are patchy, may not span the full spatial and temporal range of hatching, and produce no direct information on movements. Because tidal and net currents can transport larvae over chaotic paths and long distances (Houde 1987), survey data do not directly reflect the distribution of hatching. Methods that exploit information about the origin of individual fish include the use of thermal marks (Sahashi et al. 2015) and genetic evidence of particular parental stock (Johnson et al. 2016). Combinations of such individual-based methods have been particularly helpful in providing information on origins (Feyrer et al. 2007, 2015). Particle-tracking models (PTMs) have also been used successfully to assess dispersal of fish larvae in dynamic environments. For example, Edwards et al. (2007) used a PTM to estimate dispersal of larval fish on the US Atlantic continental shelf, inferring that spawning locations were more important than larval behavior in determining the dispersal of larvae. Sponaugle et al. (2012) used a PTM to estimate settlement rates of damselfish larvae into coral reef habitats, concluding that larval settlement was best explained by the timing of localized recruitment. PTMs have been used to infer movements of larvae collected in field surveys (Rose et al. 2013, Bauer et al. 2014) and to estimate hatching locations based on downstream catch in rivers (Embke et al. 2019). PTMs have also been embedded in individual-based models of fish populations to characterize the movements and fates of larvae (Rose et al. 2013).

The hatching distribution and subsequent movement of longfin smelt *Spirinchus thaleichthys* in the San Francisco Estuary (SFE), USA, is of great interest because of its long-term, ongoing decline in abundance. The California Department of Fish and Wildlife calculates an annual index of abundance for juvenile longfin smelt based on a trawl survey conducted in September to December of most years since 1967 (Moyle et al. 1992). The long-term trajectory of the index shows 2 major patterns: increasing abundance by 2 orders of magnitude with increasing freshwater flow, and a long-term decline of similar magnitude over the last 3 decades (Nobriga & Rosenfield 2016). The temporal decline in abundance is at least partly due to a decline in food web productivity over the same time frame (Feyrer et al. 2003, Mac Nally et al. 2010, Brown et al. 2016). Nearly 4 decades after the relationship of abundance with freshwater flow was first described (Stevens & Miller 1983) the mechanisms underlying it remain uncertain. None of the proposed mechanisms for the flow effect has been clearly shown to contribute to interannual variation (Kimmerer et al. 2013).

A particular concern is the risk of entrainment of longfin smelt larvae in large water diversions in the freshwater reach of the estuary. High estimates of this risk for the Critically Endangered delta smelt *Hypomesus transpacificus* (Kimmerer 2011, NatureServe 2014) prompted restrictions on diversion flows to reduce entrainment, which reduced this source of mortality (Smith et al. 2021). The losses of larval longfin smelt to entrainment by water diversions had not been quantified prior to this work and that of Kimmerer & Gross (2022).

Although earlier work indicated that longfin smelt spawn their adhesive eggs in fresh water (Moyle 2002), more recent analyses suggest that they may hatch in low-salinity habitats (Lewis et al. 2019). Newly hatched longfin smelt larvae are generally most abundant and may survive better in low-salinity habitats than in fresh water (Hobbs et al. 2010). Hatching largely in low-salinity habitats, instead of solely freshwater habitats, makes them less vulnerable than delta smelt to entrainment in water diversions. When freshwater flow into the SFE is high, the isohalines of the salinity field are located further seaward than in dry years (Jassby et al. 1995), and larval longfin smelt are also found further seaward (Grimaldo et al. 2017, 2020, Lewis et al. 2020). A more seaward distribution may provide more food and more habitat heterogeneity for rearing (Barros et al. 2022), and also reduces the risk of entrainment in water diversions (Grimaldo et al. 2009).

The primary objective of this study was to estimate the spatial distribution of hatching of longfin smelt during a low-flow year (2013) and a high-flow year (2017). Our method used a 3-dimensional hydrodynamic model to provide velocity information to a PTM. The PTM predicted time-varying distributions of particles representing larvae. These particles were initially seeded in candidate hatching regions of longfin smelt for hatching periods associated with discrete cohorts. A Bayesian analysis used this movement information and survey data of catch and length distributions to infer the timing and spatial distribution of hatching and estimate proportional losses of larval longfin smelt to entrainment in water-diversion facilities. All results were probabilistic, reflecting the uncertainty associated with limited catch data. A sensitivity analysis was conducted to quantify sensitivity to multiple model assumptions including the assumption of neutrally buoyant larvae and a fixed larval growth rate.

2. METHODS

2.1. Study area and species

The SFE extends from the delta of the Sacramento and San Joaquin Rivers to the Pacific Ocean (Fig. 1). The Delta is a complex network of channels in a former marsh that was long ago diked, drained, and converted to farmland. West of the Delta, the SFE consists of a series of shallow bays with deep channels, including Suisun Bay which is linked to San Pablo Bay through the narrow, deep Carquinez Strait, and Central and South San Francisco Bays. Our discussion focuses on the northern estuary, in particular San Pablo Bay to the Delta.

The SFE has mixed diurnal and semidiurnal tides with a mean tidal range of 1.25 m at the mouth of the estuary and pronounced spring–neap variability (Cheng et al. 1993). Fresh water enters the estuary mainly from the Sacramento River, and flow is widely variable among years and between the winter–spring wet season and the summer–autumn dry season. The length of salinity intrusion varies as a power function of freshwater flow, with a response time that increases from as little as 1 d to >1 mo as salt intrusion length increases (Andrews et al. 2017). The Delta is fresh during the wet season, while brackish water usually intrudes into the western Delta in summer and autumn. San Pablo Bay, Carquinez Strait, and Suisun Bay are typically partially mixed through most of the year, with stratification that varies tidally and with freshwater flow and water depth.

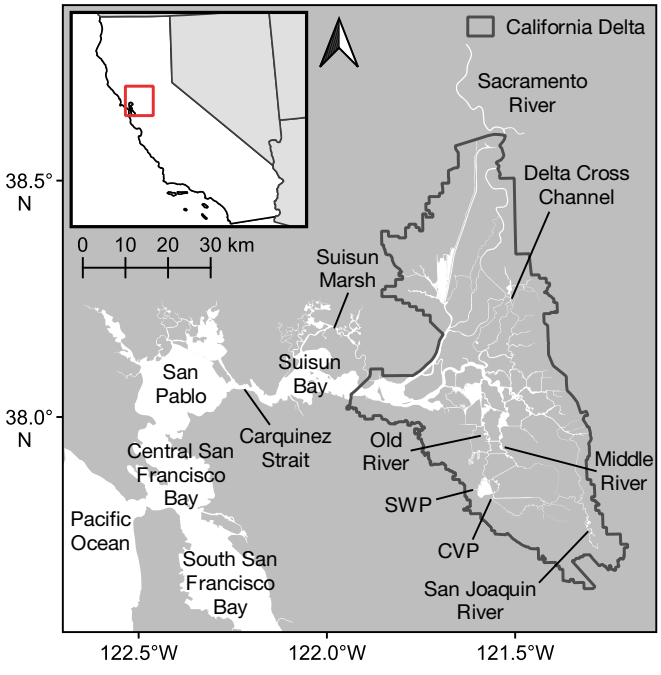

Fig. 1. Study area in the San Francisco Estuary, with key locations labeled and the extent of the California Delta shown with a grey outline. SWP: State Water Project; CVP: Central Valley Project. The location in California is shown in the inset

Massive water-development projects trap runoff in reservoirs in the wetter areas north of the SFE during winter–spring for release in the dry summer–autumn growing season, and much of the annual runoff that reaches the Delta is diverted from the southern Delta (Fig. 1) for farms and cities in the arid south. The California Department of Water Resources reports daily inflow to the Delta, diversion flows, and net Delta 'outflow', i.e. inflow less diversions and estimated consumption within the Delta.

The large diversion facilities of California's State Water Project and the federally operated Central Valley Project (Fig. 1) are equipped with louvers to separate fish from the water and return them to the estuary, but these do not work for larvae (Grimaldo et al. 2009). Losses of small fish to entrainment in the diversion flows is a major point of contention (Moyle et al. 2018).

Longfin smelt occur from southern Alaska to the SFE, mainly as anadromous populations in estuaries but also landlocked, such as in Lake Washington, USA (Chigbu & Sibley 1994, Garwood 2017, Sağlam et al. 2021). In the SFE, most adult longfin smelt spawn in shallow habitats once at 2 yr of age (Nobriga & Rosenfield 2016), primarily between January and April (Moyle 2002, Hobbs et al. 2010). Newly hatched larvae are generally found between salinities of 0 and 12, with peak observations occurring between 2 and 4 (Grimaldo et al. 2017).

2.2. Overview of approach

The analysis proceeded in 3 steps conducted separately for each year. The first step was the simulation of tidal hydrodynamics with a 3-dimensional model. The second step was to delineate several candidate regions where hatching could occur and hatching periods defining discrete cohorts, seed a PTM with particles in each hatching region and cohort throughout the associated hatching period, and determine the locations of these particles over subsequent time. The particles dispersed and moved seaward, such that at any point in the estuary particles could be present from any hatching region. The third step was the application of a Bayesian analysis to determine probabilistic daily survival and regional hatching rates during specified periods using data from 2 in-

dependent larval surveys (described in Section 2.5) and movement information from particle-tracking simulations. The analysis also estimates the proportion of the population lost to diversions based on the probability distribution of origin from each hatching region and cohort and the proportion of particles released in each region and cohort that were diverted.

In Step 1, we simulated 3-dimensional tidal hydrodynamics. The simulations ran from mid-December to May for 2013 (low-flow year, 33rd percentile of historical mean outflow over those months) and 2017 (high-flow year, 98th percentile of outflow). Flow in 2013 had 2 peaks in December and then decreased, while in 2017 flow remained elevated through the simulation period (Fig. 2). These years were chosen for availability of survey data and to span a range of freshwater inflows to the SFE.

To set up Step 2, we divided the central to northern estuary into 12 candidate hatching regions (Fig. 3) of which a subset contained larval survey stations. We designated 7 cohorts of fish that each hatched in 1 of 7 contiguous 2 wk periods spanning December to April. Hatching for the first cohort began on 9 December 2012 for the 2013 analysis and 18 December 2016 for the 2017 analysis. Particles were released hourly in

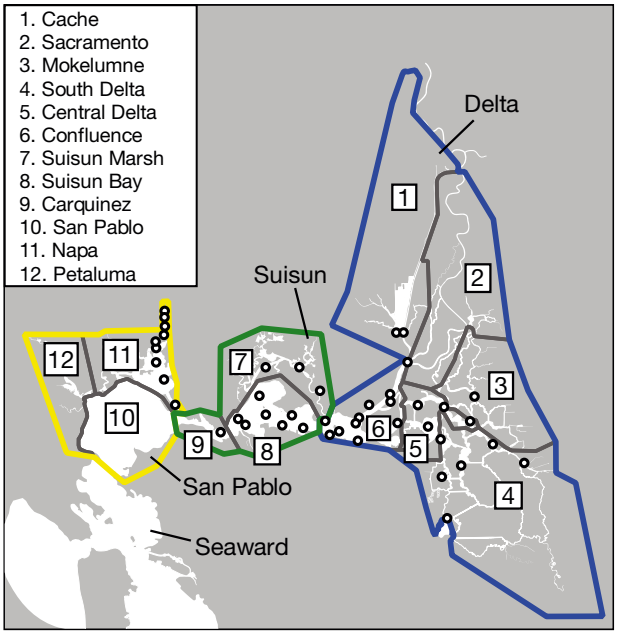

Fig. 3. Regions used in particle exchange and larval longfin smelt regional abundance estimation. The 'super-regions' discussed in later analysis are also indicated by thicker colored boundaries. Station locations for the Smelt Larva Survey are indicated with circles

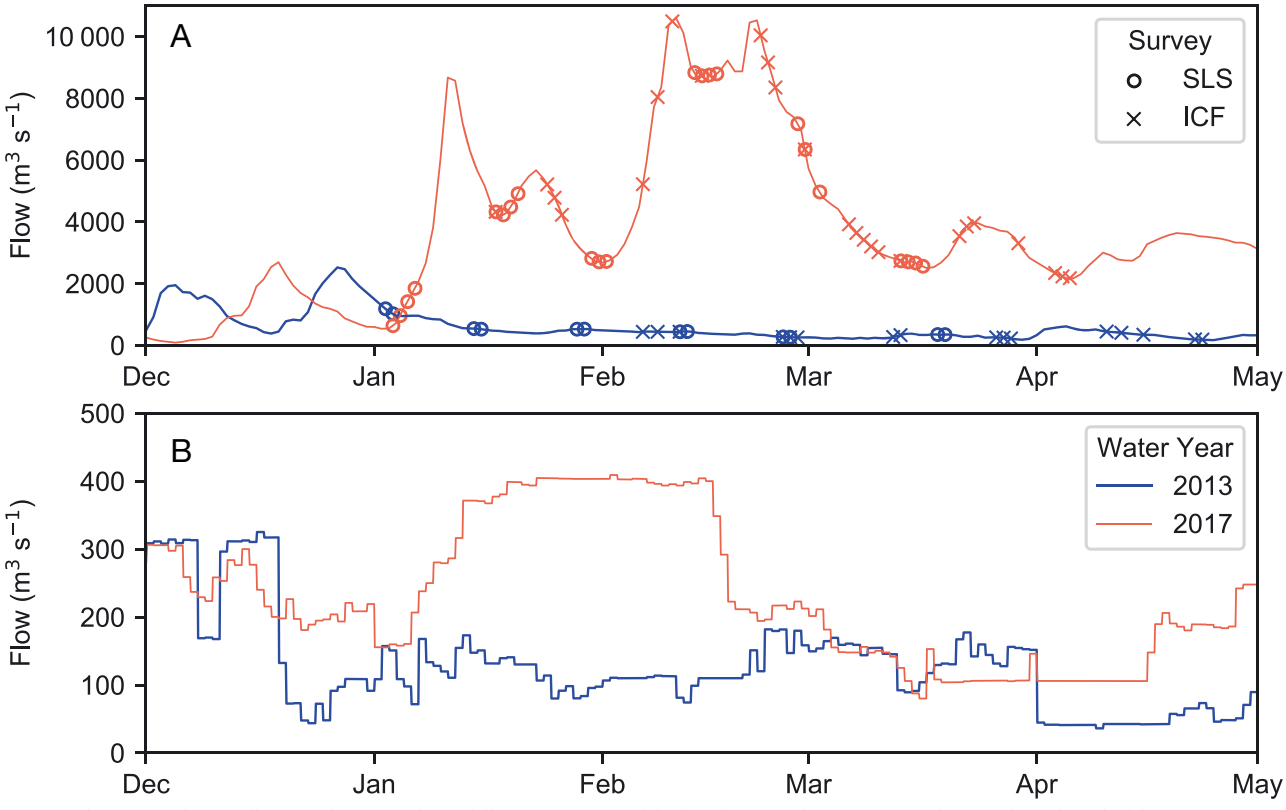

Fig. 2. (A) Net Delta outflow and (B) combined flow to state and federal water diversions in the south Delta (California Department of Water Resources, https://data.cnra.ca.gov/dataset/dayflow). Longfin smelt larvae survey dates are shown with markers in panel A (SLS: Smelt Larva Survey; ICF: International Inc. longfin smelt larva surv)

each hatching region during each 2 wk hatching period and tracked and recorded as a single cohort as they moved among recipient regions.

In Step 3, the Bayesian model was fit to catch data from the 2 larval surveys to estimate the unobserved number of larvae hatched in each cohort and hatching region, and proportional entrainment losses at the south Delta diversions. Key assumptions in our model were: (1) hatching is uniform through time for a cohort; (2) the growth rate of larvae is constant and does not vary among individuals; (3) mortality is unknown but invariant across space and time within a model run; (4) larvae behave as passive particles; (5) surveys designed to catch longfin smelt larvae are unbiased with respect to size of larvae and representative of each region; and (6) variation in catches among contemporaneous tows within a region can be represented by a negative binomial distribution.

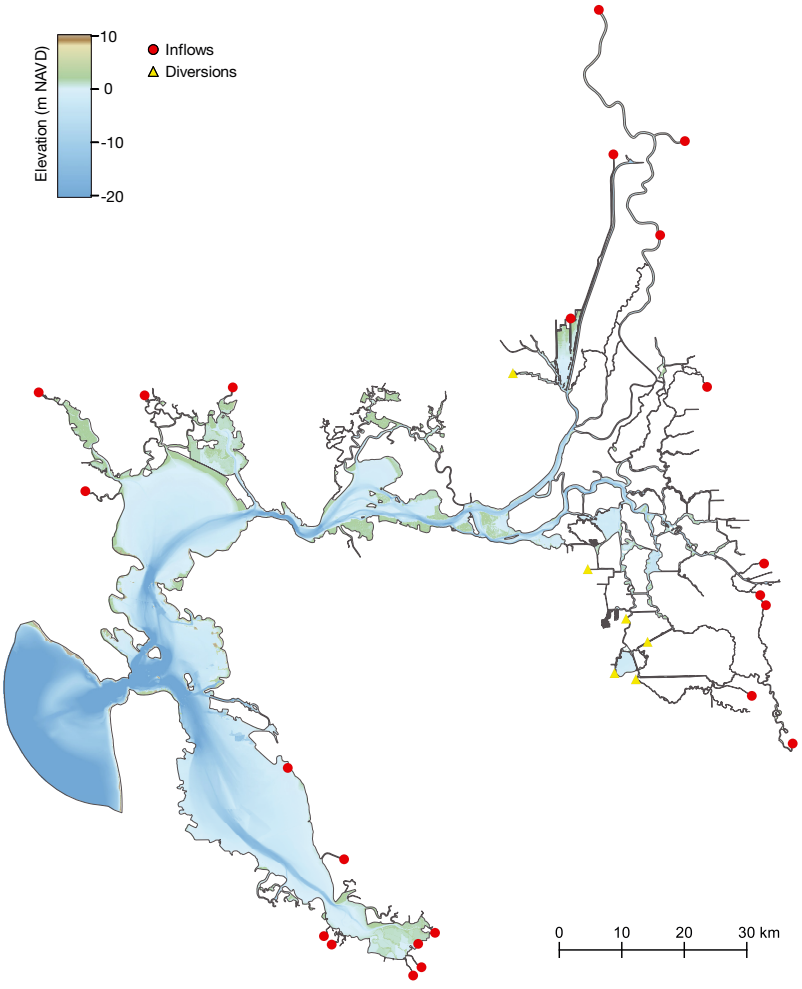

Fig. 4. Resource Management Associates UnTRIM San Francisco Estuary model: extent of domain, bathymetry, and location of key freshwater inputs and diversions. NAVD: North American Vertical Datum

2.3. Hydrodynamic model

UnTRIM (Casulli & Walters 2000, Casulli & Stelling 2011) is a 3-dimensional numerical hydrodynamic model that solves the Reynolds-averaged Navier-Stokes equations on an unstructured horizontal grid, and allows subgrid-scale representation of bathymetry. The Resource Management Associates (RMA) UnTRIM San Francisco Estuary model has been applied in several studies (Andrews et al. 2017, Gross et al. 2019) with a model domain extending from the Pacific Ocean through the SFE (Fig. 4).

The model was calibrated against water level, flow, and salinity data gathered during the 2 model periods at continuous-monitoring locations through the estuary (Gross et al. 2019, Kimmerer et al. 2019). Average hydrodynamic model skill scores (Willmott 1981) reported by Kimmerer et al. (2019) for water level, flow, and salinity were 0.974, 0.957, and 0.847, respectively.

2.4. PTM

The PTM calculates 3-dimensional particle trajectories using distributions of velocity and eddy diffusivity from the hydrodynamic simulations (Ketefian et al. 2016). The instantaneous and time-averaged trajectories of particles can vary widely between neutrally buoyant (passive) particles and those that either sink or move vertically in synchrony with tidal currents (Kimmerer et al. 2014). Based on field observations, yolk-sac larvae of longfin smelt appear to be initially surface-oriented but move throughout the water column after ~10 mm length, and fish larger than ~16 mm may undergo tidal vertical migration (Bennett et al. 2002). Weakly buoyant particles in well-mixed and weakly salinity-stratified regions of the estuary had similar horizontal distributions to passive particles (unpublished results in model runs described by Kimmerer et al. 2014). Therefore, we used passive particles for this study, which resulted in a vertically well-mixed distribution, consistent with the results of Bennett et al. (2002) for larvae of 10–16 mm length. We also explored the sensitivity of

results to this assumption by repeating the particle-tracking simulation for surface-oriented particles that were distributed in the upper 3.5 m of the water column, consistent with the observations of Bennett et al. (2002) for larvae smaller than ~10 mm length. In this simulation, each individual particle was assigned a distance from the surface between zero and 3.5 m drawn from a uniform random distribution and retained this fixed distance from the surface through the simulation period.

In the 2013 simulation, we released particles in each of the 9 candidate hatching regions landward of San Pablo Bay (Fig. 3), consistent with the extent of larval surveys in 2013. Seven cohorts were defined, each spanning a 2 wk interval. Particles were released hourly with a uniform number of particles per area through each of 9 candidate hatching regions, resulting in 63 groups of particles tracked in 2013. Roughly 2 million total particles were tracked in the 2013 simulation.

Freshwater flow was much higher in 2017 than in 2013 (Fig. 2), and the salinity field and larval distribution were shifted seaward. For the 2017 simulation, survey data were available in San Pablo Bay and adjacent tidal sloughs. Therefore, 3 candidate hatching regions in San Pablo Bay (Fig. 3) were included in the 2017 simulation, resulting in a total of 12 candidate hatching regions.

Transport of particles representing larvae was summarized as the daily proportion in each region of larvae in each cohort that originated from each hatching region, which is conceptually similar to a set of 'connectivity matrices' (Paris et al. 2007). We also calculated the daily proportion of particles from each hatching region that were entrained into the water diversions in the south Delta.

2.5. Bayesian analysis

The California Department of Fish and Wildlife began the Smelt Larva Survey (SLS) in 2009 to assess the vulnerability of longfin smelt larvae to entrainment at the water-diversion facilities in the southern Delta. The SLS in 2013 and 2017 consisted of 6 surveys at roughly 2 wk intervals (Fig. 2). In each survey, a single tow was conducted at each of 44 stations from Carquinez Strait into the Delta (Fig. 3). Nine stations in the Napa River (Fig. 3) were sampled in 2017 but not in 2013. The SLS samples were collected by 10 min stepped-oblique tows from near the bottom to the surface, using a 500 µm mesh net with a mouth area of 0.37 m^2 (Mitchell et al. 2019), for a typical tow volume of 200 m^3. Additional data were collected ('ICF' survey, ICF International Inc., https://www.icf.com/) using similar gear on several dates during 6 February through 23 April 2013 and 12 January through 13 March 2017 (Fig. 2; Grimaldo et al. 2017). Both surveys reported catch and fork length of either all longfin smelt caught or a subsample of 50 fish.

Larval smelt were assigned to model cohorts based on their hatch date, which was estimated from length data together with size at hatch and estimated growth rate. Two empirical approaches for estimating growth rate were used to provide a range of values for use in analyses (see Section S1 in the Supplement available at www.int-res.com/articles/suppl/m700p179_supp.pdf). (1) Growth rates of cultured larvae of known age were estimated from the distribution of length at age. (2) *In situ* grow rates of wild larvae (collected in field surveys) were estimated using established otolith-based aging protocols (Hobbs et al. 2007, Xieu et al. 2021). Growth rates were modeled as the slopes of linear size–age relationships for each group of fish (Wang 2007). Results suggested that mean larval growth rates could reasonably vary from 0.15 to 0.22 mm d^{-1}, with a mean growth rate of 0.19 mm d^{-1}, consistent with previous otolith-based growth estimates of larval longfin smelt (Lewis et al. 2019) (Table S2). The mean observed length at hatch was 6.2 mm.

We predicted abundance in each cohort for each region and day as a function of the number of that cohort previously hatched in each source region, daily survival, and the movement information determined by the PTM:

$$N_{n,i,d} = e^{\gamma_n}\Phi(\phi,d,s_n)\sum_{j}^{nsources}\theta_{n,j}\lambda_{n,j,i,d}\beta_{n,d-s_n} \quad (1)$$

where $N_{n,i,d}$ is abundance (total number) of cohort n in region i on day d, e^{γ_n} is the number of larvae hatched in cohort n across all regions, $\Phi(\phi,d)$ is the average survival of the cohort from hatching to day d, where the survival on day d of the subset of larvae in the cohort which hatched on the first day is ϕ^{d-s_n}, ϕ is the daily survival rate, s_n is the first day of hatching of cohort n, *nsources* is the number of candidate hatching regions (9 for 2013, 12 for 2017), and $\theta_{n,j}$ is the fraction of cohort n hatched in hatching region j (variables are defined in Table 1). The regional movement predicted by the PTM is represented by $\lambda_{n,j,i,d}$, the fraction of particles in cohort n hatched in region j that are in region i on day d, and $\beta_{n,d-s_n}$ is the fraction of fish in cohort n that are in the larval life stage on day d. The particle-tracking approach treats larvae as passive particles, which applies to larvae smaller than ~16 mm as discussed in Section 2.4. It is

Table 1. Definitions of variables

Term	Definition
n	Cohort index
i	Recipient region index
d	Day index
j	Hatching region index
k	Tow index
γ_n	Log-transformed number of larvae hatched in cohort n
Φ	Average survival across all larvae in a cohort
ϕ	Daily survival
s_n	Start time of hatching of cohort n
$\theta_{n,j}$	Fraction of cohort n hatched in hatching region j
$\lambda_{n,j,i,d}$	Fraction of particles in cohort n hatched in region j that are in region i on day d
nsources	Number of hatching regions (9 in 2013, 12 in 2017)
nreg	Number of regions (12)
ncohorts	Number of cohorts (6)
ndiv	Number of diversions (2)
$\beta_{n,d-s_n}$	Fraction of fish in cohort n that remain larvae on day d
$N_{i,d}$	Regional abundance of larvae in region i on day d
C_k	Observed catch (no. of fish) for tow k
V_k	Volume of tow k (m^3)
$\tilde{V}_i$	Water volume in region i (m^3)
α	Overdispersion parameter of negative binomial distribution (1.106)
$\tilde{\boldsymbol{C}}_k$	Vector of observed measured catch in each cohort for tow k
$\hat{\boldsymbol{f}}_{i,d}$	Fraction of abundance in each cohort for region i and day d corresponding to tow k
M_k	Measured catch (no. of fish) for tow k
P_d	Proportional losses on day d

also possible that larvae grow large enough to avoid the gear. For these reasons, we limited our analysis to larvae smaller than 16 mm, which takes 52 d with the assumed hatch length of 6.2 mm and growth rate of 0.19 mm d^{-1}. Therefore, $\beta_{n,d-s_n} = 1$ from the beginning of hatching through Day 52 and then linearly decreases to reach zero after 14 more days, when the last larvae in the cohort reach 16 mm. The total larval abundance in region i on day d, $N_{i,d}$, is the sum of abundances across all cohorts.

We constructed a statistical model comparing observed and predicted catch in each region and survey:

$$C_k \sim negbin\left(N_{i,d} \times \frac{V_k}{\tilde{V}_i}, \alpha\right) \quad (2)$$

where C_k is observed catch for tow k, V_k is the tow volume, $N_{i,d}$ is total predicted abundance of larvae of all cohorts in region i and day d for tow k, $\tilde{V}_i$ is the water volume in region i, *negbin* is a negative binomial distribution, and α is the overdispersion parameter ($\alpha = 0$ makes this a Poisson distribution). Note that $N_{i,d} \times \frac{V_k}{\tilde{V}_i}$ is an estimate of expected catch for tow k in region i. Eq. (2) was also used in an independent analysis to estimate the overdispersion parameter α from 2013 catch data, resulting in a value of 1.106. In that analysis, we used all catch data in each region to fit probabilistic estimates of regional abundance for each survey and an overdispersion parameter (α) that applies to all regions and surveys.

The total catch (C_k) can include larvae from multiple cohorts. The proportion of each cohort in the total catch was estimated using a multinomial distribution:

$$\tilde{\boldsymbol{C}}_k \sim \text{multinominal}\,(\hat{\boldsymbol{f}}_{i,d}, M_k) \quad (3)$$

where **bold** font is used to indicate a vector quantity spanning all cohorts, $\tilde{\boldsymbol{C}}_k$ is a vector of measured catch attributable to each cohort for tow k, $\hat{\boldsymbol{f}}_{i,d}$ is a vector giving the proportion of predicted abundance in each cohort from tow k in region i and day d, and M_k is the number of fish caught in tow k that were measured, which may be smaller than C_k because not all captured fish were measured.

The model predicted the regional hatching distribution for each candidate hatching region and cohort ($\theta_{n,j}$), the number of larvae hatched for each cohort (e^{γ_n}), and daily survival (ϕ) which applies to all cohorts, for a total of 71 parameters for 2013. The minimally informative prior probability distributions used in the fitting were:

$$\gamma_n = \mathcal{U}(0.1, 30) \quad (4)$$

$$\sum_{j}^{nsources} \theta_{n,j} = ddirch(1:nsources) \quad (5)$$

$$\phi = dbeta(1,1) \quad (6)$$

where $\mathcal{U}$ is a uniform distribution over the specified range, *ddirch* is a Dirichlet distribution, and *dbeta* is a beta distribution.

The values of the hatching and survival parameters were estimated in JAGS 4.3.0 (Plummer 2017) using 3 independent Markov chains of 100 000 samples per chain after a burn-in period of 10 000 samples to minimize the influence of initial conditions. Ten-fold thinning was used to reduce the total number of samples in the posterior distributions for each parameter to 30 000. The parameters for hatching distribution and survival were fit separately for each year. The Bayesian model converged for both years. The Gelman-Rubin convergence diagnostic was less than 1.005 for all parameters in both years, indicating that the model run was long enough for the 3 Markov chains for each parameter to converge (Gelman et al. 2003). Some autocorrelation of samples was observed in chains, but the statistics of the first and second half of

samples in each chain were nearly identical, indicating that the burn-in and sample length were adequate.

2.6. Proportional losses to entrainment

The proportional loss of larvae to entrainment in water diversions was calculated from:

$$P_d = \sum_{l}^{ndiv} \sum_{n}^{ncohorts} \frac{e^{\gamma_n}}{\sum e^{\gamma_n}} \sum_{j}^{nsources} \theta_{n,j} \sum_{d'}^{d} (\lambda_{n,j,l,d} - \lambda_{n,j,l,d'}) \beta_{n,d-s_n} \quad (7)$$

where P_d are cumulative proportional entrainment losses up to day d, $ndiv$ is the number of diversion locations, and $\lambda_{n,j,l,d}$ is the part of the movement information indicating the fraction of particles representing larvae hatched in cohort n and region j that have been entrained by water diversion l up to day d. $\beta_{n,d-s_n}$ is the portion of hatched fish from cohort n that are less than 16 mm length on day d. P_d is equal to one minus the ratio of the extant population to the population that would have existed in the absence of entrainment.

3. RESULTS

3.1. Smelt larva surveys

The total catch per unit effort at each station summed across the 6 surveys in 2013 was highest in Suisun Bay and the confluence of the Sacramento and San Joaquin Rivers (Fig. 5A). The observed length of the fish had a sharp peak at 7 mm. Catches were much lower in the higher flow year of 2017 (Fig. 5B), and most stations in the Delta had zero catch during 2017, likely due to dispersal of larvae further downstream beyond the SLS sampling area (Grimaldo et al. 2020). We focus most of the analysis and discussion on 2013 (a dry year) because fish are more likely to hatch and remain within the sampling area during drier years, and the subsequently higher catches made parameters more identifiable and less uncertain than was possible with the 2017 data.

ICF surveys sampled mostly in Suisun Bay in 2013 and from San Pablo Bay through Suisun Bay in 2017 (Grimaldo et al. 2020). Length distributions were similar between the ICF and SLS surveys (Fig. 5).

3.2. Particle movements

The PTM predicted tidal and net movement from each combination of hatching region and cohort. An example distribution of particles from a single cohort (5) and hatching region (Confluence) on the last day of the cohort's hatching period (Fig. 6) gives a rough picture of the cumulative movements of this set of 18 000 particles released during the hatching period in 2013. The number of particles in a single recipient region divided by the total number released in the

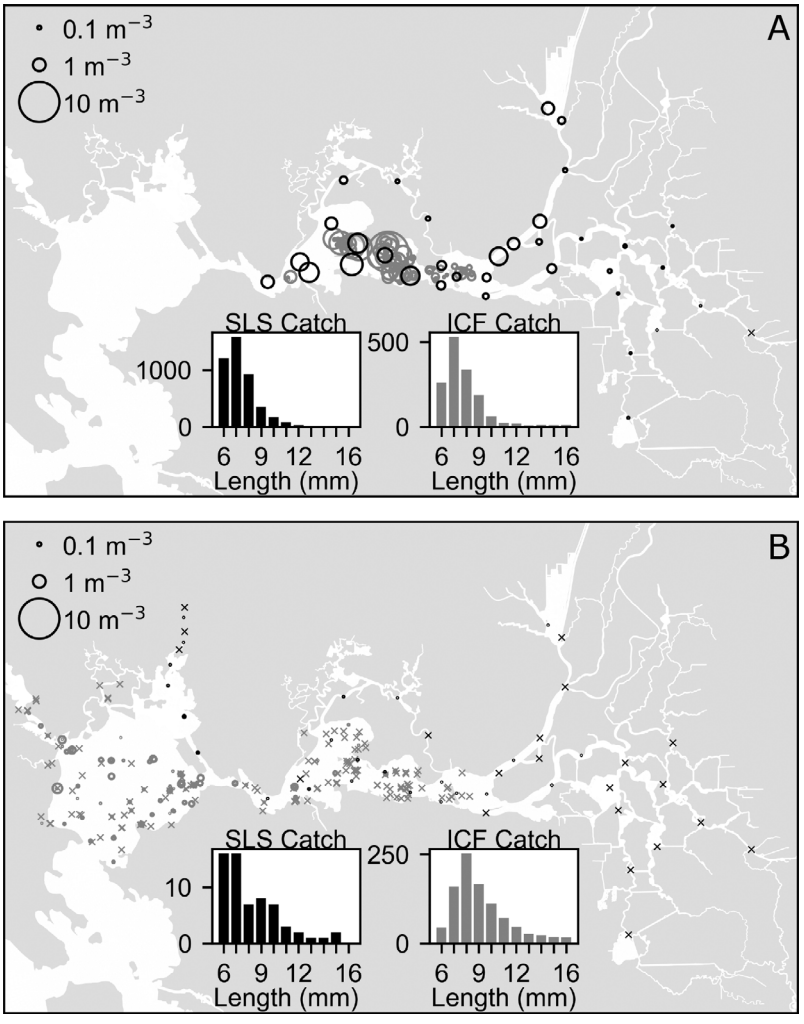

Fig. 5. Catch per unit effort (CPUE) of longfin smelt larvae (m^{-3}) averaged across 6 Smelt Larva Survey (SLS) surveys shown in black circles and ICF International Inc. data for individual trawls in grey circles, both with circle area proportional to CPUE, for (A) 2013 and (B) 2017. The '×' symbol indicates zero catch at a station. Inset histograms for each year show no. of fish by length for SLS data (black) and ICF data (grey)

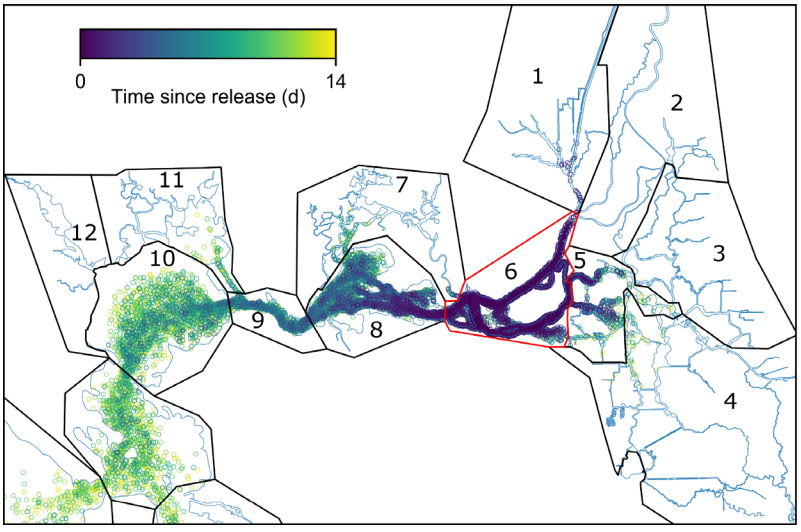

Fig. 6. Distribution of particles (circles) from cohort 5 and region 6 (red outline) on 24 February 2013, the last day of hatching for cohort 5. Colors of circles correspond to days since release. Regions as in Fig. 3

hatching region gives $\lambda_{n,j,i,d}$ (Eq. 1) for the cohort, hatching region, recipient region, and day of the simulation. This process of counting particles in each region was repeated for each cohort, hatching region, and recipient region on each day of the simulation to calculate all $\lambda_{n,j,i,d}$. The calculated $\lambda_{n,j,i,d}$ is summarized in Fig. 7 for the end of the 2 wk hatching period of each cohort, using the 4 larger 'super-regions' outlined in Fig. 3 instead of the 12 smaller recipient regions to simplify the graph. At the end of the hatching interval for each cohort, the larvae associated with that cohort ranged in size from 6.2 to 8.9 mm, which includes the mode of the size distribution of total observed catch (Fig. 5). Therefore, the data in Fig. 7 are representative of the amount of movement between hatching and the collection of catch data used in the Bayesian model. The amount of movement varied among cohorts, with cohort 1 moving further seaward than other cohorts because of higher flow during that early period (Fig. 2). Consistent with the distribution of particles in Fig. 6, the movement was primarily in the seaward direction because of seaward net flow. However, this does not imply that tidal dispersion or estuarine circulation processes were weak. A large amount of dispersion is evident in the wide geographic distribution of particles in Fig. 6 and the distribution information in Fig. 7.

3.3. Hatching distribution and daily survival

The estimated hatching distribution was centered on Suisun Bay (Fig. 8). The posterior estimates of hatching distribution were negatively correlated between some pairs of adjoining regions, notably the Suisun Bay and Confluence regions, which is reflected in somewhat wide interquartile ranges for some hatching rate estimates for these candidate hatching regions (Figs. 8 & 9). The temporal peak of estimated hatching was cohort 5, which hatched from 10 to 24 February 2013.

The estimated total hatching in 2017 (4.7 billion) was smaller than in 2013 (11.8 billion) and distributed seaward (west) of the distribution in 2013 (Fig. 9). Most hatching occurred in San Pablo Bay (region 10) and the Petaluma River (region 12). The hatching distribution estimates for 2017 were based on far lower catch than 2013 (Fig. 5). The low catch and high frequency of zeros limit confidence in the hatching magnitude and distribution estimated for 2017, but the distribution was clearly seaward of that in 2013 (Fig. 9).

The daily survival estimated for 2013 was 0.964 with a 90% credible interval of 0.955–0.971. The estimate for 2017 was 0.9997 with a 90% credible interval of 0.9987–1.0000.

3.4. Entrainment losses

The predicted number of larvae entrained from each hatching region varied greatly with proximity of the hatching region to the South Delta (Fig. 10), and entrainment from candidate hatching regions west of the Confluence (region 6) was negligible. Although few larvae hatched in the South Delta (Fig. 8), a large fraction of those were entrained (Fig. 7), so they contributed the most to entrainment (Fig. 10). In contrast, Suisun Bay had the most hatching (Fig. 8), but few larvae from Suisun Bay were entrained (Fig. 10).

Estimated total entrainment in water diversions removed a minor proportion of the population (Fig. 11). These results suggest that losses to diversions comprised a 1.95% decrease in larval population (90% credible intervals 1.2–3.12%) in 2013, and losses were negligible in 2017. The daily survival parameter for 2013 of 0.964 corresponds to 14.9% survival over the 52 d larval period. If entrainment losses could have been eliminated, estimated survival of larvae to the juvenile life stage in 2013 would have increased to 15.2%.

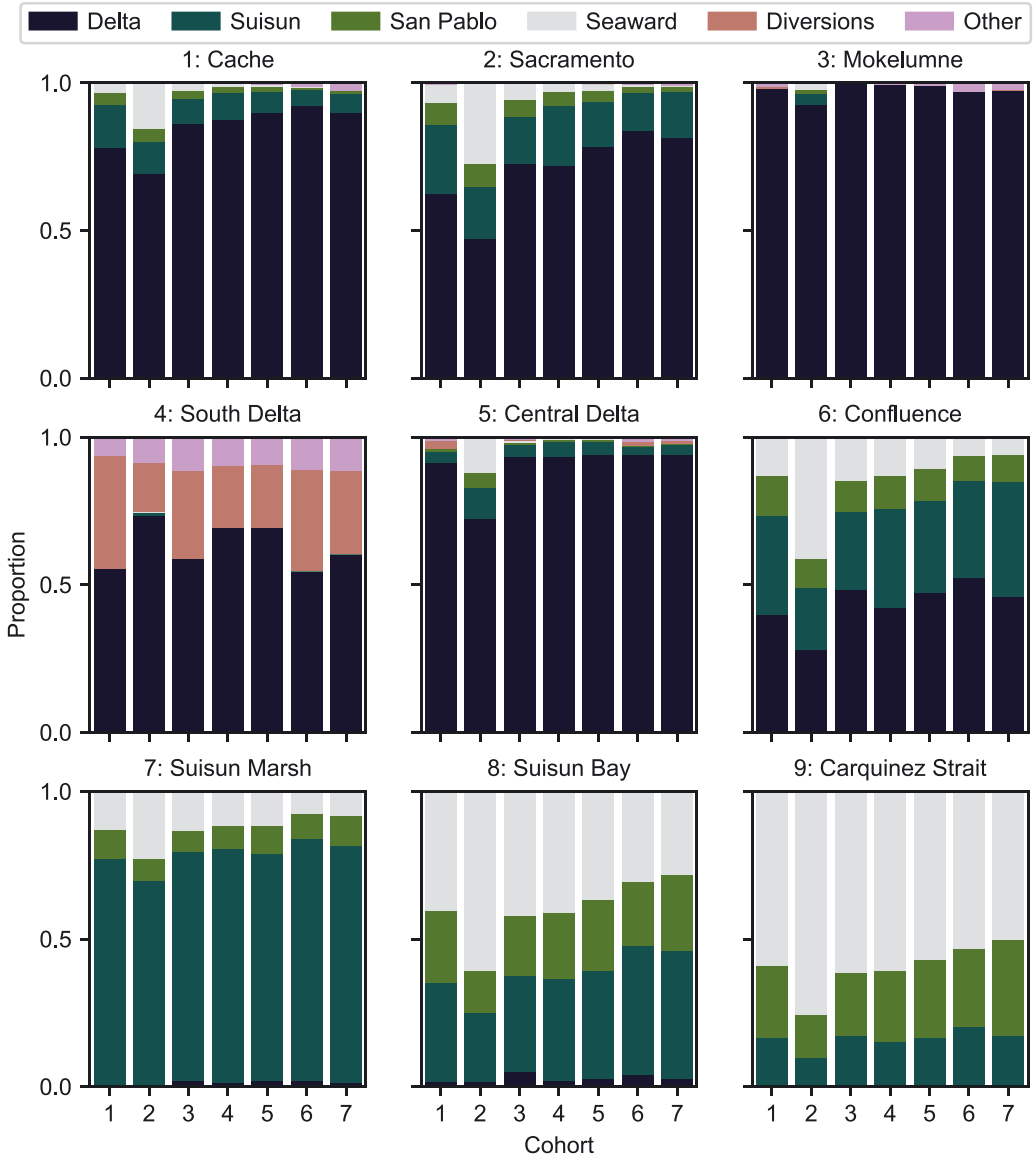

Fig. 7. Distributions of particles from each release region (see Fig. 3) at the end of the 2 wk hatching period for each cohort (*x*-axis). Bar segments indicate proportions of particles in each super-region. The 'Other' category (in purple) includes agricultural and other small diversions in the Delta

3.5. Sensitivity analysis

The analysis included an estimated growth rate based on observed length-at-age data for wild longfin smelt, and an overdispersion parameter estimated from 2013 SLS catch data. We explored the sensitivity of predictions to these parameters by refitting the model to the observations for a range of growth rates and overdispersion parameters (Table 2). The range of

Table 2. Sensitivity of key metrics to assumed parameters for 2013. The first row gives results from the baseline run

Growth rate (mm d^{-1})	α	Hatching (billions)	Vertical distribution	Fraction hatched in Delta	Survival (d^{-1})	Proportional entrainment losses
0.19	1.106	11.8	Well-mixed	0.385	0.964	0.0195
0.15	1.106	8.57	Well-mixed	0.508	0.975	0.0285
0.22	1.106	17.8	Well-mixed	0.623	0.924	0.0218
0.19	0.935	11.9	Well-mixed	0.365	0.964	0.0155
0.19	1.304	11.8	Well-mixed	0.403	0.963	0.0247
0.19	1.106	13.1	Surface	0.336	0.958	0.0111

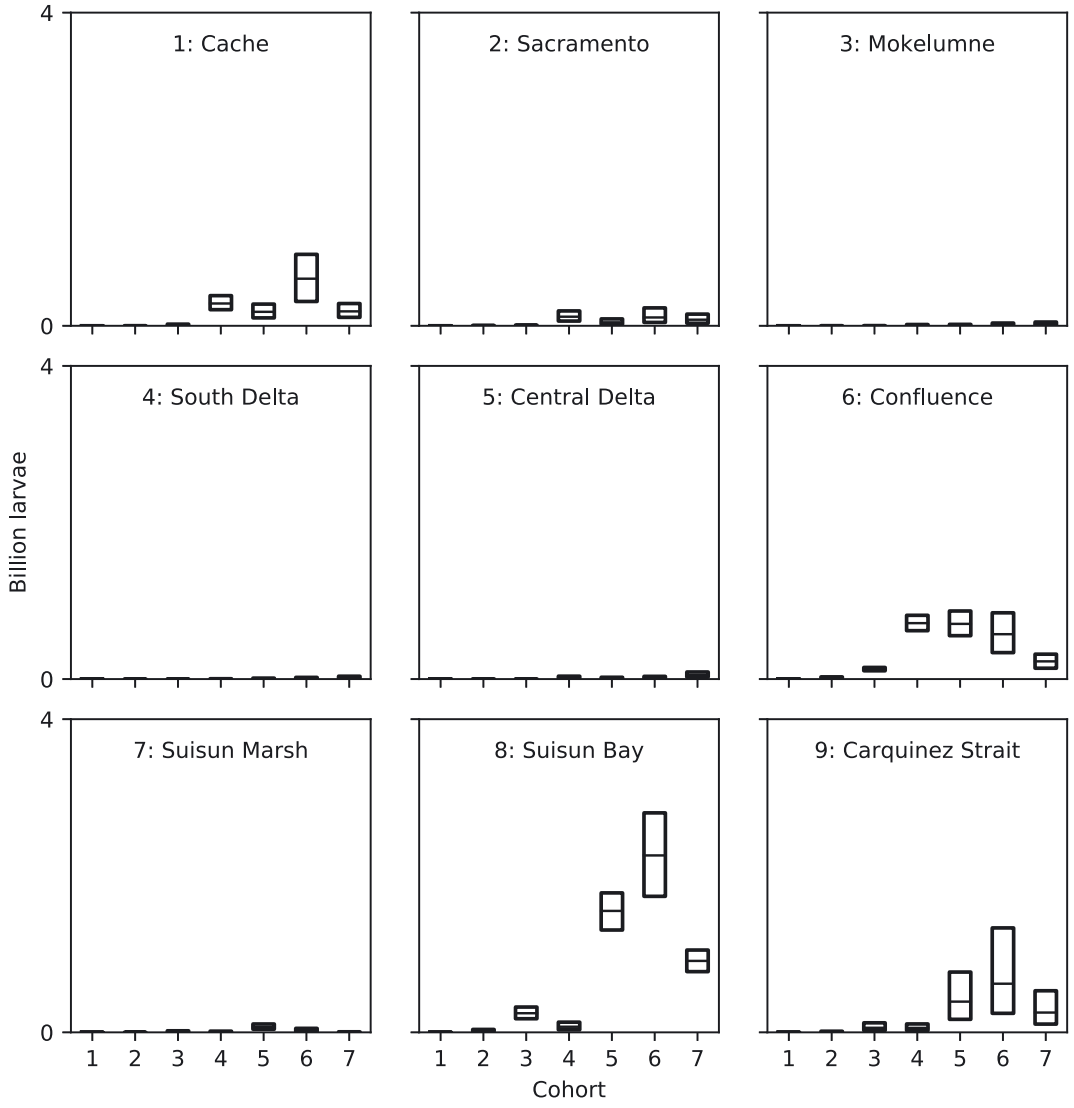

Fig. 8. Boxes showing median and interquartile range of number hatched for each combination of hatching region (see Fig. 3) and cohort (*x*-axis)

growth rate spans the range of observed mean growth rates of cultured longfin smelt larvae and mean growth rates of wild fish estimated using otolith-based techniques (Fig. S1). The 5 to 95% credible limits of the overdispersion parameter were (0.935, 1.304).

The range of estimated growth rates led to changes in all parameters, with higher growth rates leading to increased estimated number of larvae hatched. Entrainment for both growth rate sensitivity tests were within the 90% credible intervals of the medium entrainment estimates estimated for the assumed growth rate of 0.19 mm d^{-1}. Increasing α led to a larger proportion of estimated hatching in the Delta and higher estimated proportional entrainment losses. The increase in α indicates less confidence that observed catch is representative of actual density of larvae. The results using a low α of 0.935 reflect increased confidence in catch data and, therefore, more hatching in Suisun Bay where the majority of catch was observed in 2013. In the surface-oriented particle simulation, predicted hatching increased and entrainment decreased (Table 2).

4. DISCUSSION

Our key findings are that longfin smelt hatch further seaward than previously believed (Moyle 2002), which makes them less vulnerable to entrainment in the water diversion facilities than believed. This entrainment has been shown to cause substantial mortality to the Critically Endangered delta smelt in

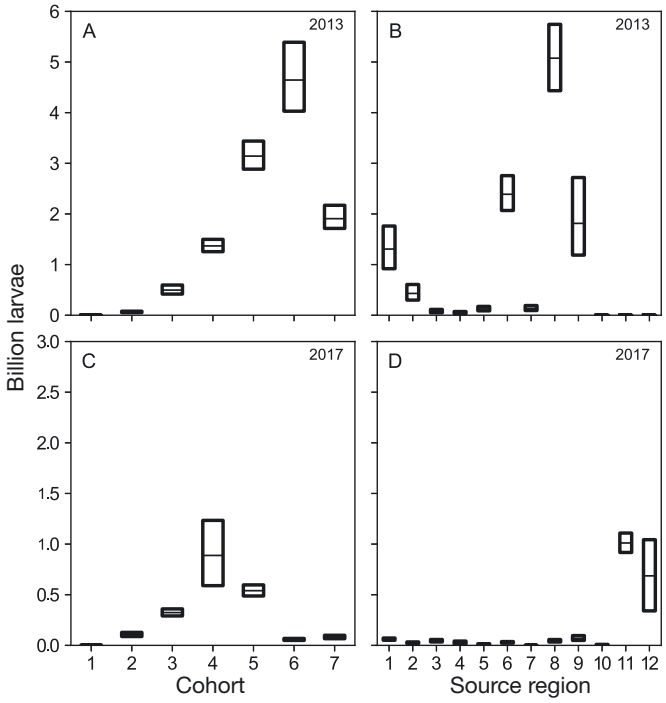

Fig. 9. Median and interquartile range of larvae hatched in each (A,C) cohort and (B,D) hatching region (see Fig. 3) in 2013 (A,B) and 2017 (C,D). Note scale differences between the 2 years

some years (Kimmerer 2008, 2011, Smith et al. 2021), adding to contention about the diversion of fresh water from this tidal estuary (Moyle et al. 2018). In contrast to delta smelt, our analysis indicates that entrainment of larval longfin smelt does not have substantial effects on the population. The principal reason for this difference is that delta smelt spawn and larvae develop further landward, with a greater proportion in fresh water, than longfin smelt (Wang 2007, Hobbs et al. 2010, 2019, Lewis et al. 2019).

The estimated daily survival of larvae for 2013 was 0.964, which corresponds to a daily mortality of 0.037. No other estimates of mortality are available for longfin smelt. An individual-based model of delta smelt used a value of 0.05 d^{-1} for larvae past the yolk-sac stage, and the value for yolk-sac larvae, used as a tuning parameter to get the overall abundance close to estimates from surveys, was 0.035 d^{-1} (Rose et al. 2013). A state-space model of delta smelt yielded a mean daily mortality of early post-larvae (May–June) of 0.04 d^{-1} (Smith et al. 2021, W. Smith pers. comm.). Thus, the survival estimate for 2013 was in the right range for similar-sized larvae of an osmerid in the same estuary.

The novelty of our approach for estimating larval movement lies in the use of results from a PTM in a Bayesian model that was fit to catch data to estimate temporal and spatial distributions of hatching. Here we provide context for our results: first we discuss the general topic of larval transport and settlement, then ways of assessing transport, and then turn to the specific case study of longfin smelt.

4.1. Larval transport

Planktonic larvae of fish and invertebrates differ qualitatively from their juvenile and adult stages in being more affected by the vagaries of transport from where they hatch to where they develop (Pineda et al. 2007). The planktonic larvae of some invertebrate taxa have a similar potential for dispersal to that of larval fish (Bradbury & Snelgrove 2001). Despite strong effects of dispersal, planktonic larvae can recruit to suitable rearing habitats after traveling over long distances (e.g. reef fish, Cowen et al. 2006, Paris et al. 2007) or between estuaries and adjacent oceans (Epifanio & Garvine 2001), generally by behaviors that amplify the probability of reaching these habitats.

The limited swimming ability of larvae constrains the mechanisms available for movement to a particular habitat or region. The literature on larval movement illustrates that a wide variety of larval types use a rich array of mechanisms for directed movements in currents that greatly exceed their swimming speed (Bradbury & Snelgrove 2001). Generally, these mechanisms take advantage of features of the 4-dimensional flow field such as persistent or ephemeral vertical and lateral shears, retention zones, tidal oscillations, wind shear, and seasonal reversals (Wing et al. 1998, Epifanio & Garvine 2001, Largier 2003, Morgan et al. 2014). Probably the best-known mechanism for small planktonic organisms to move against strong currents is selective tidal stream transport by which the organisms leave the water column during unfavorable currents, effectively ratcheting their way against the unfavorable currents (Forward & Tankersley 2001, Simons et al. 2006). A related mechanism is tidally oriented vertical or lateral migration, which is effective in sheared tidal currents even when the observed vertical movements are subtle (Kimmerer et al. 1998, 2014, Kunze et al. 2013). Larvae may swim vertically to enter depth zones of favorable large-scale currents such as to exit offshore surface currents in upwelling areas (Paris et al. 2007), or to move toward regions likely to offer suitable substrate.

Variability at the intersection between transport processes and larval behavior means that success of larvae in recruiting to suitable rearing habitat can be highly variable in time and space (Cowen et al. 2006). The enormous risk of failure of an individual

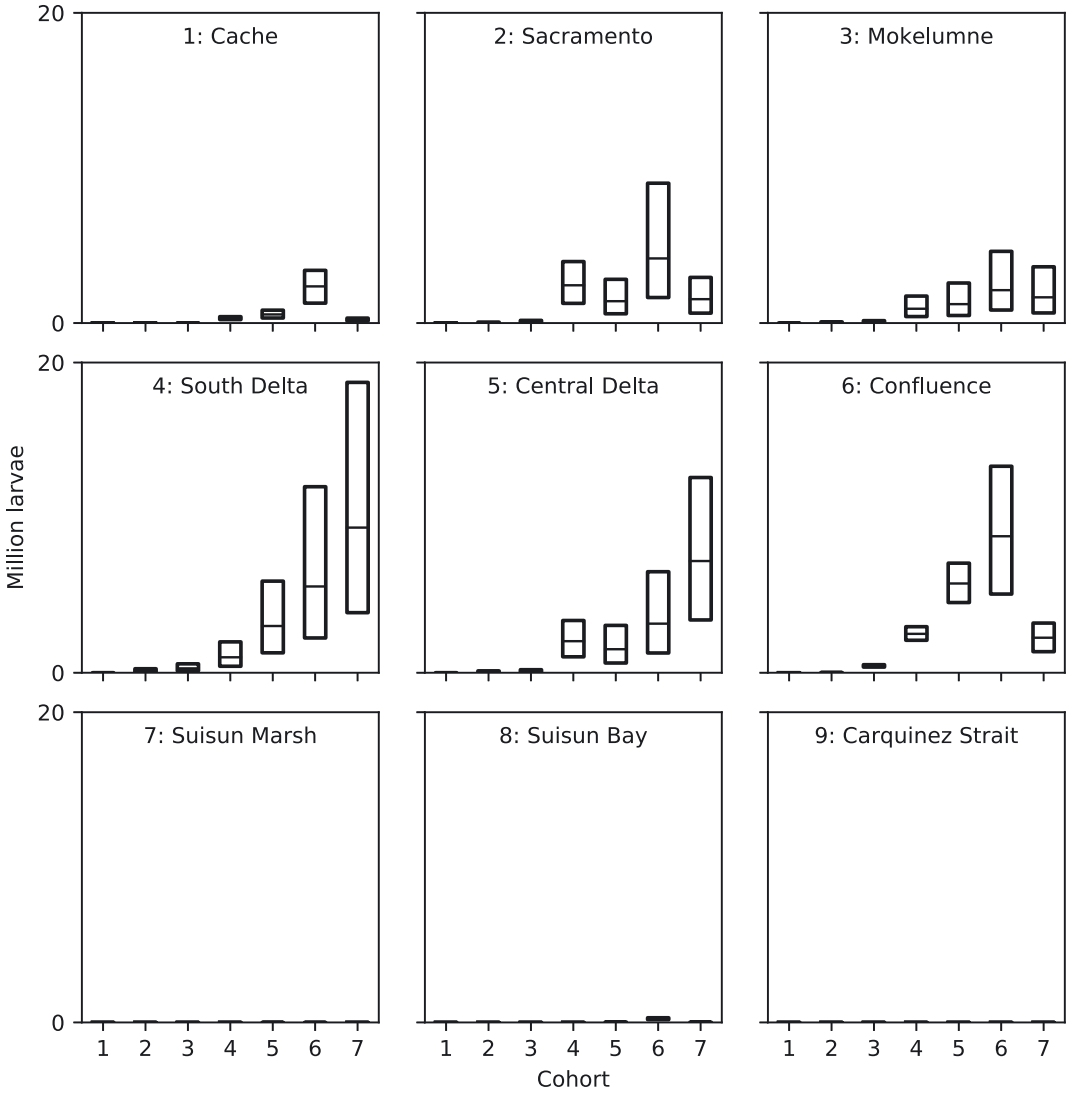

Fig. 10. Median and interquartile range of larvae entrained in water diversions in the southern Delta, from each combination of hatching region (see Fig. 3) and cohort (*x*-axis)

larva is suggested by the massive outpouring of propagules of many benthic and fish species with planktonic life stages (Cowen et al. 2006, Pineda et al. 2007). Benthic organisms may settle in a small subset of available habitat and under a limited set of physical-oceanographic conditions (Pineda et al. 2007).

Larval longfin smelt are faced with a particular challenge. The behavior of early larvae is likely passive, and our PTM with passive behavior gives a reasonable fit to the distribution of larval longfin smelt. While many of the particles representing larvae moved out of the study area, later larvae are found most abundantly in the low-salinity reach of the estuary (Kimmerer et al. 2013). This implies a transition between passive and directional behavior that may include tidal vertical migration (suggested by the data of Bennett et al. 2002) and depth-seeking behavior. However, the SLS monitoring data include no information about vertical position, nor information about larval distribution seaward of Carquinez Strait.

4.2. Modeling transport

A lot has been learned about transport and dispersion of planktonic organisms through theoretical efforts such as those pioneered by Okubo (1978, 1986, 1994). These efforts continue to provide a basis for understanding how transport depends on the interaction of advective and dispersive processes with the behaviors of larvae (Largier 2003). Though essential

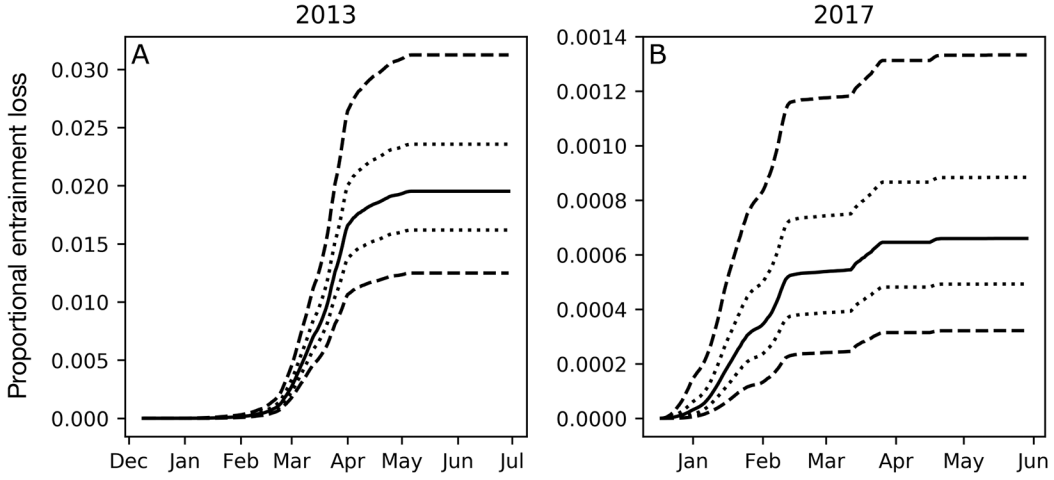

Fig. 11. Estimated median cumulative proportional entrainment of larvae for (A) 2013 and (B) 2017 with 5 and 95% credible intervals shown with dashed lines and 25 and 75% credible intervals shown with dotted lines

for developing understanding, these approaches are limited in their applicability for quantifying hatching distribution and timing.

Advances in computer capabilities and in the sophistication and speed of hydrodynamic models and PTMs have led to rapid advances in investigations of larval transport in which model predictions are confronted with observations from the field. Many such modeling efforts have used dispersal kernels to represent statistically the spread of larvae with time and distance from an initial site (Siegel et al. 2003, Edwards et al. 2007, Sponaugle et al. 2012). These approaches may be uncertain in coastal environments with complex flow fields such as estuaries and very near shore, where interactions can be highly nonlinear and transport can be influenced by small-scale processes not well parameterized as dispersion.

Alternatively, explicit particle tracking can be used to represent the movements of individual organisms to investigate their distribution through time, as we have done. This general approach has been used in comparisons of settlement patterns of reef fish with detailed observations (Sponaugle et al. 2012), and individual-based modeling of larval (Rose et al. 2013) and adult fish (Korman et al. 2021).

Particle-tracking approaches can be coupled with methods of assessing the actual locations of the organisms. When comparing expected catch from a modeling approach to observed catch, it is essential to take into consideration the inherent variability in count data. Typically counts of organisms collected in the field must be modeled explicitly using an underlying statistical distribution appropriate to the data; we used a negative binomial distribution to represent the overdispersed statistical distribution of the larvae. Our Bayesian analytical framework included all of the available survey data from each study year, thereby providing parameter estimates with their full likelihoods, which allowed us to draw robust conclusions about hatching distribution and survival.

4.3. Hatching and transport of longfin smelt

The distributions of particles during model runs (Fig. 6) show that if larvae truly behaved passively, most of them would have been swept far seaward of the sampling area. That is, passive behavior would preclude retention of most larvae in the estuary, especially under high flows. Yet, some fraction of the population either remains in, or returns to, low-salinity habitat during development, and the resulting population size is higher under high than under low flows (Nobriga & Rosenfield 2016).

Particles that sink or migrate tidally can be retained in low-salinity regions of the estuary, particularly in stratified regions from Carquinez Strait to the ocean (Kimmerer et al. 2014). Tidal migration and distribution of longfin smelt larger than ~16 mm deeper in the water column (Bennett et al. 2002) improve retention in this region of active estuarine circulation (Kimmerer et al. 2014). Ongoing work is applying ontogenetic development of sinking and tidal migration to explore retention of longfin smelt during transition between late larvae and juveniles, similar to work done previously for copepods (Kimmerer et al. 2014).

Results of this study are conditional on the assumptions of the model, including constant mortality, fixed

growth rate, and no size selectivity of gear. Since these 3 factors are interrelated, growth rate and gear selectivity as parameters would be unidentifiable or highly uncertain. Growth rate is well constrained by available data, and size selectivity is unlikely to be strong for larvae in the 6–16 mm size range (Mitchell et al. 2019).

Some other factors not included in the model may be important; in particular, catches of larval and juvenile longfin smelt are inversely related to water clarity (Thomson et al. 2010), a pattern that has been widely observed at a variety of scales (Heege & Appenzeller 1998). Evidence from a variety of sources supports several mechanisms for this pattern, none mutually exclusive: the fish may be consumed at a higher rate in clear water (Gregory & Levings 1998), they may avoid or reduce their foraging activities in clear water (Utne-Palm 2002), or sampling efficiency may be reduced in clear water (McGurk 1992). Each of these mechanisms implies a different outcome in a study such as ours, but we are unable to resolve these with the modeling tools now available, nor have the necessary behavioral studies of longfin smelt been conducted to inform modeling.

Based on our analysis, the hatching distribution was centered on Suisun Bay in 2013, with some hatching in the Confluence and Cache Slough regions and negligible hatching elsewhere in the Delta (Fig. 9). Surprisingly, hatching in Suisun Marsh contributed little to the population, although high larval abundance has previously been reported there (Wang 2007). This seeming disparity is partially a result of the small area and volume of water in Suisun Marsh (~10% of the volume in Suisun Bay).

For the wet winter–spring of 2017, our results suggest that longfin smelt predominantly hatched within San Pablo Bay and associated tidal sloughs. This result is consistent with the negligible catch of longfin smelt in the SLS survey while the ICF survey caught numerous longfin smelt in San Pablo Bay (Fig. 5). Hatching seaward of San Pablo Bay could not be constrained with the available catch data (Fig. 5), and substantial hatching may occur in South San Francisco Bay as well (Grimaldo et al. 2020, Lewis et al. 2020). It remains unclear what spawning habitats, substrates, and conditions are necessary for spawning by longfin smelt (Wang 2007). It also remains unclear how closely hatch locations match spawning locations. Fertilized eggs of longfin smelt are known to disperse with currents and to hatch away from original spawning locations (Grimaldo et al. 2017). In 2017, longfin smelt were estimated to have hatched in tidal sloughs or freshwater tributaries of San Pablo Bay (e.g. Petaluma River, Sonoma Creek, and Napa River), with newly-hatched larvae dispersed downstream into San Pablo Bay by high flows. However, reproductively mature longfin smelt were rarely observed in these habitats during monthly surveys from 2015 to 2019 (Lewis et al. 2019).

Previous reports have inferred that longfin smelt spawn mainly in fresh waters of the Delta (Moyle 2002, Hobbs et al. 2010). This assumption was based loosely on the distribution of adult and larval fish, and was likely influenced by previous work on the landlocked population in Lake Washington (Moulton 1974). By contrast, our results indicate that a significant fraction of larvae may hatch and develop further seaward than previously believed, which is consistent with conceptual models (Nobriga & Rosenfield 2016) and field observations (Grimaldo et al. 2020) that suggest hatching of longfin smelt in San Pablo Bay and Lower South Bay during wet years.

Although some temporal changes in the distribution of larvae have recently been described (Eakin 2021), it is likely that historical larval distributions have included seaward locations wherever suitable habitat occurs (Wang 2007, Nobriga & Rosenfield 2016). For example, recent studies of longfin smelt physiology (Yanagitsuru et al. 2022) and otolith geochemistry (Lewis et al. 2019) have confirmed successful hatching and rearing in low-salinity habitats that are broadly distributed seaward in winter–spring of wet years. The potential importance of these habitats has resulted in mandates to extend several monitoring programs (e.g. California Department of Fish and Wildlife SLS, 20 mm, and trawl surveys) throughout the estuary, including open-water, tributary, and wetland habitats of San Pablo Bay and South San Francisco Bay (California Department of Water Resources 2020).

Our results suggest that interannual variation in losses of longfin smelt larvae to diversions during hatching and development in spring are not large enough to meaningfully alter a 100-fold interannual range in the abundance index determined the following autumn (Kimmerer et al. 2009). Comparisons of hatch distributions and proportional entrainment among years spanning a greater variety of outflow and environmental conditions could shed further light on the direct effects of diversions on this imperiled fish. A companion study (Kimmerer & Gross 2022) partially accomplished this goal by estimating population size of larval longfin smelt and entrainment losses using a simpler approach over a 12 yr period. Results from that study showed that entrainment losses were low in all years, and results for 2013 and 2017 were consistent with those presented here.

Acknowledgements. We thank Richard Rachiele for guidance on model calibration and Rusty Holleman for providing python tools for analysis of model results. Vincenzo Casulli developed the UnTRIM hydrodynamic model. Steve Andrews led the development of the RMA UnTRIM interface and associated analysis code. Longfin smelt monitoring data were provided by the California Department of Fish and Wildlife. The UC Davis Fish Conservation and Culture Facility provided known-age specimens for aging, and the staff of the Otolith Geochemistry & Fish Ecology Laboratory provided wild specimens and conducted otolith analyses. Funding was provided by the California Department of Fish and Wildlife under agreement #P1696013 to San Francisco State University. Viewpoints expressed in this manuscript are those of the authors and do not reflect the opinions of the California Department of Water Resources.

LITERATURE CITED

Andrews SW, Gross ES, Hutton PH (2017) Modeling salt intrusion in the San Francisco Estuary prior to anthropogenic influence. Cont Shelf Res 146:58–81

Barros A, Hobbs JA, Willmes M, Parker CM and others (2022) Spatial heterogeneity in prey availability, feeding success, and dietary selectivity for the threatened longfin smelt. Estuar Coast 45:1766–1779

Bauer RK, Gräwe U, Stepputtis D, Zimmermann C, Hammer C (2014) Identifying the location and importance of spawning sites of Western Baltic herring using a particle backtracking model. ICES J Mar Sci 71:499–509

Bennett WA, Kimmerer WJ, Burau JR (2002) Plasticity in vertical migration by native and exotic estuarine fishes in a dynamic low-salinity zone. Limnol Oceanogr 47:1496–1507

Bradbury IR, Snelgrove PVR (2001) Contrasting larval transport in demersal fish and benthic invertebrates: the roles of behaviour and advective processes in determining spatial pattern. Can J Fish Aquat Sci 58:811–823

Bradbury IR, Snelgrove PVR, Fraser S (2000) Transport and development of eggs and larvae of Atlantic cod, *Gadus morhua*, in relation to spawning time and location in coastal Newfoundland. Can J Fish Aquat Sci 57:1761–1777

Bradbury IR, Gardiner K, Snelgrove PVR, Campana SE, Bentzen P, Guan L (2006) Larval transport, vertical distribution, and localized recruitment in anadromous rainbow smelt (*Osmerus mordax*). Can J Fish Aquat Sci 63: 2822–2836

Brown LR, Kimmerer W, Conrad JL, Lesmeister S, Mueller-Solger A (2016) Food webs of the Delta, Suisun Bay, and Suisun Marsh: an update on current understanding and possibilities for management. San Franc Estuary Watershed Sci 14:4

California Department of Water Resources (2020) Longfin smelt science plan 2020–2030. https://water.ca.gov/-/media/DWR-Website/Web-Pages/Programs/State-Water-Project/Files/ITP/ITP-Longfin-Science-Plan_SWP_12232020_-FINAL.pdf

Casulli V, Stelling GS (2011) Semi-implicit subgrid modelling of three-dimensional free-surface flows. Int J Numer Methods Fluids 67:441–449

Casulli V, Walters RA (2000) An unstructured grid, three-dimensional model based on the shallow water equations. Int J Numer Methods Fluids 32:331–348

Cheng RT, Casulli V, Gartner JW (1993) Tidal, residual, intertidal mudflat (TRIM) model and its applications to San Francisco Bay, California. Estuar Coast Shelf Sci 36: 235–280

Chigbu P, Sibley TH (1994) Relationship between abundance, growth, egg size and fecundity in a landlocked population of longfin smelt, *Spirinchus thaleichthys*. J Fish Biol 45:1–15

Cowen RK, Paris CB, Srinivasan A (2006) Scaling of connectivity in marine populations. Science 311:522–527

Eakin M (2021) Assessing the distribution and abundance of larval longfin smelt: What can a larval monitoring program tell us about the distribution of a rare species? California Fish and Wildlife Special CESA Issue 107:189–202. https://nrm.dfg.ca.gov/FileHandler.ashx?DocumentID=193402&inline

Edwards KP, Hare JA, Werner FE, Seim H (2007) Using 2-dimensional dispersal kernels to identify the dominant influences on larval dispersal on continental shelves. Mar Ecol Prog Ser 352:77–87

Embke HS, Kocovsky PM, Garcia T, Mayer CM, Qian SS (2019) Modeling framework to estimate spawning and hatching locations of pelagically spawned eggs. Can J Fish Aquat Sci 76:597–607

Epifanio CE, Garvine RW (2001) Larval transport on the Atlantic continental shelf of North America: a review. Estuar Coast Shelf Sci 52:51–77

Feyrer F, Herbold B, Matern SA, Moyle PB (2003) Dietary shifts in a stressed fish assemblage: consequences of a bivalve invasion in the San Francisco Estuary. Environ Biol Fishes 67:277–288

Feyrer F, Nobriga ML, Sommer TR (2007) Multidecadal trends for three declining fish species: habitat patterns and mechanisms in the San Francisco Estuary, California, USA. Can J Fish Aquat Sci 64:723–734

Feyrer F, Hobbs J, Acuna S, Mahardja B and others (2015) Metapopulation structure of a semi-anadromous fish in a dynamic environment. Can J Fish Aquat Sci 72:709–721

Forward RB, Tankersley RA (2001) Selective tidal-stream transport of marine animals. Oceanogr Mar Biol Annu Rev 39:305–353

Garwood RS (2017) Historic and contemporary distribution of longfin smelt (*Spirinchus thaleichthys*) along the California coast. Calif Fish Game 103:96–117

Gelman A, Carlin JB, Stern HS, Rubin DB (2003) Bayesian data analysis, 2nd edn. CRC, Boca Raton, FL

Gregory RS, Levings CD (1998) Turbidity reduces predation on migrating juvenile Pacific salmon. Trans Am Fish Soc 127:275–285

Grimaldo LF, Sommer T, Van Ark N, Jones G and others (2009) Factors affecting fish entrainment into massive water diversions in a tidal freshwater estuary: Can fish losses be managed? N Am J Fish Manag 29:1253–1270

Grimaldo L, Feyrer F, Burns J, Maniscalco D (2017) Sampling uncharted waters: examining rearing habitat of larval longfin smelt (*Spirinchus thaleichthys*) in the upper San Francisco Estuary. Estuar Coast 40:1771–1784

Grimaldo L, Burns J, Miller RE, Kalmbach A, Smith A, Hassrick J, Brennan C (2020) Forage fish larvae distribution and habitat use during contrasting years of low and high freshwater flow in the San Francisco Estuary. San Franc Estuary Watershed Sci 18:6

Gross E, Andrews S, Bergamaschi B, Downing B, Holleman R, Burdick S, Durand J (2019) The use of stable isotope-based water age to evaluate a hydrodynamic model. Water 11:2207

Heege T, Appenzeller A (1998) Correlations of large-scale

patterns of turbidity and pelagic fish biomass using satellite and acoustic methods. Arch Hydrobiol Spec Issue 53: 489–503

Hobbs JA, Bennett WA, Burton JE, Baskerville-Bridges B (2007) Modification of the biological intercept model to account for ontogenetic effects in laboratory-reared delta smelt (*Hypomesus transpacificus*). Fish Bull 105:30–38

Hobbs JA, Lewis LS, Ikemiyagi N, Sommer T, Baxter RD (2010) The use of otolith strontium isotopes ($^{87}Sr/^{86}Sr$) to identify nursery habitat for a threatened estuarine fish. Environ Biol Fishes 89:557–569

Hobbs JA, Lewis LS, Willmes M, Denney C, Bush E (2019) Complex life histories discovered in a critically endangered fish. Sci Rep 9:16772

Houde ED (1987) Fish early life dynamics and recruitment variability. Am Fish Soc Symp 2:17–29

Jassby AD, Kimmerer WJ, Monismith SG, Armor C and others (1995) Isohaline position as a habitat indicator for estuarine populations. Ecol Appl 5:272–289

Johnson RC, Garza JC, MacFarlane RB, Grimes CB and others (2016) Isotopes and genes reveal freshwater origins of Chinook salmon *Oncorhynchus tshawytscha* aggregations in California's coastal ocean. Mar Ecol Prog Ser 548:181–196

Ketefian GS, Gross ES, Stelling GS (2016) Accurate and consistent particle tracking on unstructured grids. Int J Numer Methods Fluids 80:648–665

Kimmerer WJ (2008) Losses of Sacramento River Chinook salmon and delta smelt to entrainment in water diversions in the Sacramento-San Joaquin Delta. San Fran Estuar Watershed Sci 6

Kimmerer WJ (2011) Modeling delta smelt losses at the south Delta export facilities. San Franc Estuary Watershed Sci 9:3

Kimmerer WJ, Gross ES (2022) Population abundance and diversion losses in a threatened estuarine pelagic fish. Estuar Coast https://doi.org/10.1007/s12237-022-01101-w

Kimmerer WJ, Burau JR, Bennett WA (1998) Tidally-oriented vertical migration and position maintenance of zooplankton in a temperate estuary. Limnol Oceanogr 43: 1697–1709

Kimmerer WJ, Gross ES, MacWilliams M (2009) Is the response of estuarine nekton to freshwater flow in the San Francisco Estuary explained by variation in habitat volume? Estuar Coast 32:375–389

Kimmerer WJ, MacWilliams ML, Gross ES (2013) Variation of fish habitat and extent of the low-salinity zone with freshwater flow in the San Francisco Estuary. San Franc Estuary Watershed Sci 11: 1

Kimmerer WJ, Gross ES, MacWilliams ML (2014) Tidal migration and retention of estuarine zooplankton investigated using a particle-tracking model. Limnol Oceanogr 59:901–916

Kimmerer W, Wilkerson F, Downing B, Dugdale R and others (2019) Effects of drought and the emergency drought barrier on the ecosystem of the California Delta. San Franc Estuary Watershed Sci 17:2

Korman J, Gross E, Grimaldo L (2021) Statistical evaluation of behavior and population dynamics models predicting movement and proportional entrainment loss of adult delta smelt in the Sacramento–San Joaquin River Delta. San Franc Estuary Watershed Sci 19:1

Kunze HB, Morgan SG, Lwiza KM (2013) Field test of the behavioral regulation of larval transport. Mar Ecol Prog Ser 487:71–87

Largier JL (2003) Considerations in estimating larval dispersal distances from oceanographic data. Ecol Appl 13: 71–89

Lewis L, Barros A, Willmes M, Denney C and others (2019) Interdisciplinary studies on longfin smelt in the San Francisco Estuary. 2018–19 Annual Report for DWR Contract # 4600011196. Prepared for: California Department of Water Resources & IEP Longfin Smelt Technical Team. University of California, Davis

Lewis LS, Willmes M, Barros A, Crain PK, Hobbs JA (2020) Newly discovered spawning and recruitment of threatened longfin smelt in restored and underexplored tidal wetlands. Ecology 101:e02868

Mac Nally R, Thomson JR, Kimmerer WJ, Feyrer F and others (2010) An analysis of pelagic species decline in the upper San Francisco Estuary using multivariate autoregressive modelling (MAR). Ecol Appl 20:1417–1430

McGurk MD (1992) Avoidance of towed plankton nets by herring larvae: a model of night–day catch ratios based on larval length, net speed and mesh width. J Plankton Res 14:173–181

Mitchell L, Newman K, Baxter R (2019) Estimating the size selectivity of fishing trawls for a short-lived fish species. San Franc Estuary Watershed Sci 17:5

Morgan SG, Fisher JL, McAfee ST, Largier JL, Miller SH, Sheridan MM, Neigel JE (2014) Transport of crustacean larvae between a low-inflow estuary and coastal waters. Estuar Coast 37:1269–1283

Moulton LL (1974) Abundance, growth, and spawning of the longfin smelt in Lake Washington. Trans Am Fish Soc 103:46–52

Moyle PB (2002) Inland fishes of California, 2nd edn. University of California Press, Berkeley, CA

Moyle PB, Herbold B, Stevens DE, Miller LW (1992) Life history and status of the delta smelt in the Sacramento–San Joaquin Estuary, California. Trans Am Fish Soc 121:67–77

Moyle PB, Hobbs JA, Durand JR (2018) Delta smelt and water politics in California. Fisheries 43:42–50

NatureServe (2014) Delta smelt *Hypomesus transpacificus* (errata version published in 2020). The IUCN Red List of Threatened Species 2014: e.T10722A174778740

Nobriga ML, Rosenfield JA (2016) Population dynamics of an estuarine forage fish: disaggregating forces driving long-term decline of longfin smelt in California's San Francisco Estuary. Trans Am Fish Soc 145:44–58

Okubo A (1978) Horizontal dispersion and critical scales for phytoplankton patchiness. In: Steele JH (ed) Spatial pattern in plankton communities. Plenum, New York, NY, p 21–42

Okubo A (1986) Dynamical aspects of animal grouping: swarms, schools, flocks, and herds. Adv Biophys 22:1–94

Okubo A (1994) The role of diffusion and related physical processes in dispersal and recruitment of marine populations. In: Sammarco PW, Heron ML (eds) The biophysics of marine larval dispersal. Coastal and Estuarine Studies 45. American Geophysical Union, Washington, DC, p 5–32

Paris CB, Cherubin LM, Cowen RK (2007) Surfing, spinning, or diving from reef to reef: effects on population connectivity. Mar Ecol Prog Ser 347:285–300

Pineda J, Hare JA, Sponaugle S (2007) Larval transport and dispersal in the coastal ocean and consequences for population connectivity. Oceanography 20:22–39

Plummer M (2017) JAGS Version 4.3.0 user manual. https://sourceforge.net/projects/mcmc-jags/

Rose KA, Kimmerer WJ, Edwards KP, Bennett WA (2013) Individual-based modeling of delta smelt population dynamics in the upper San Francisco Estuary. I. Model description and baseline results. Trans Am Fish Soc 142: 1238–1259

Sağlam İK, Hobbs J, Baxter R, Lewis LS, Benjamin A, Finger AJ (2021) Genome-wide analysis reveals regional patterns of drift, structure, and gene flow in longfin smelt (*Spirinchus thaleichthys*) in the northeastern Pacific. Can J Fish Aquat Sci 78:1793–1804

Sahashi G, Morita K, Ohnuki T, Ohkuma K (2015) An evaluation of the contribution of hatchery stocking on population density and biomass: a lesson from masu salmon juveniles within a Japanese river system. Fish Manag Ecol 22:371–378

Siegel DA, Kinlan BP, Gaylord B, Gaines SD (2003) Lagrangian descriptions of marine larval dispersion. Mar Ecol Prog Ser 260:83–96

Simons RD, Monismith SG, Johnson LE, Winkler G, Saucier FJ (2006) Zooplankton retention in the estuarine transition zone of the St. Lawrence Estuary. Limnol Oceanogr 51:2621–2631

Smith WE, Polansky L, Nobriga ML (2021) Disentangling risks to an endangered fish: using a state-space life cycle model to separate natural mortality from anthropogenic losses. Can J Fish Aquat Sci 78:1008–1029

Sponaugle S, Paris C, Walter KD, Kourafalou V, D'Alessandro E (2012) Observed and modeled larval settlement of a reef fish to the Florida Keys. Mar Ecol Prog Ser 453: 201–212

Stevens DE, Miller LW (1983) Effects of river flow on abundance of young chinook salmon, American shad, longfin smelt, and delta smelt in the Sacramento–San Joaquin River system. N Am J Fish Manag 3:425–437

Thomson JR, Kimmerer WJ, Brown LR, Newman KB and others (2010) Bayesian change point analysis of abundance trends for pelagic fishes in the upper San Francisco Estuary. Ecol Appl 20:1431–1448

Utne-Palm AC (2002) Visual feeding of fish in a turbid environment: physical and behavioural aspects. Mar Freshw Behav Physiol 35:111–128

Wang JCS (2007) Spawning, early life stages, and early life histories of the osmerids found in the Sacramento–San Joaquin Delta of California. US Department of the Interior Bureau of Reclamation, Mid-Pacific Region, Denver, CO

Willmott CG (1981) On the validation of models. Phys Geogr 2:184–194

Wing SR, Botsford LW, Ralston SV, Largier JL (1998) Meroplanktonic distribution and circulation in a coastal retention zone of the northern California upwelling system. Limnol Oceanogr 43:1710–1721

Xieu W, Lewis LS, Zhao F, Fichman RA and others (2021) Experimental validation of otolith-based age and growth reconstructions across multiple life stages of a critically endangered estuarine fish. PeerJ 9:e12280

Yanagitsuru YR, Daza IY, Lewis LS, Hobbs JA, Hung TC, Connon RE, Fangue NA (2022) Growth, osmoregulation, and ionoregulation of longfin smelt (*Spirinchus thaleichthys*) yolk-sac larvae at different salinities. Conserv Physiol 10:coac041

Editorial responsibility: Steven Morgan, Bodega Bay, California, USA
Reviewed by: C. B. Woodson and 2 anonymous referees

Submitted: December 10, 2021
Accepted: August 26, 2022
Proofs received from author(s): October 17, 2022